Journal of Materials Chemistry C

ROYAL SOCIETY OF CHEMISTRY

PAPER

View Article Online
View Journal | View Issue

Cite this: J. Mater. Chem. C, 2025, 13, 17300

Enhancing the reversibility of thermochromism of polydiacetylene-based nanostructures embedded in a natural polymer matrix†

Karolina Bieniaś,[ab] Piotr Wieczorek,[ab] Tomasz Uchacz,*[a] Alicja Fryc,[a] Angelika Kmita,[c] Xueling Feng,[de] Peiyi Wu[de] and Szczepan Zapotoczny*[a]

We propose an approach to enhance the reversibility of thermochromism in polydiacetylene-based nanostructures, which are known for switching between blue and red colors in response to temperature variations. It was achieved by derivatizing 10,12-pentacosadiynoic acid (PCDA) and embedding the formed self-assembled nanoplatelets in an alginate matrix prior to photopolymerization that leads to a thermochromic 2D conjugated system. Amide groups were introduced to PCDA by reacting with (*N*-aminoethyl)acetamide to strengthen the network of hydrogen bonds between the molecules that enabled the formation of stable bilayer nanosheets as imaged by AFM and verified by molecular modeling. The use of alginate as a polymer matrix significantly improved the stability and reversibility of the thermochromism of dispersed PCDA-based nanosheets likely due to the formation of hydrogen bonds between them and alginate chains. The best reversibility of the thermochromic behavior was obtained in 0.001% alginate aqueous medium as followed with bare eyes and quantified using colorimetric response calculated as the level of recovery of the blue band ("percent blue", PB = 44%). Gelation of the system with Ca^{2+} ions increased the reversibility to PB = 68% due to immobilization and separation of the nanoplatelets in the polymer matrix that was further improved after drying to reach PB = 70%. The resulting nanocomposites combine high stability with the ability to respond to thermal stimuli in a controlled manner, making it an attractive system for applications in colorimetric sensors and smart polymer materials including fibers where reversible thermochromic properties are highly desired.

Received 21st March 2025,
Accepted 2nd July 2025

DOI: 10.1039/d5tc01233c

rsc.li/materials-c

Introduction

Thermochromism is a phenomenon that, among other applications, has the potential for the fabrication of fluorescent and colorimetric sensors for detecting biologically and chemically important molecules,[1,2] electro-thermochromic displays,[3] anti-counterfeiting materials[4] or smart fibers.[5,6] Conjugated polymers can exhibit this phenomenon due to the presence of delocalized π electrons along the macromolecular backbone, which have the ability to transduce signals, which gives them desirable properties for use in optoelectronics and colorimetric sensors.[7] Polydiacetylenes (PDA), first described by Wegner in 1969,[8] are a type of highly conjugated polymers that undergo chromatic responses upon exposure to a variety of environmental stimuli, such as pH,[9] heat,[10] solvent,[11,12] light,[13] mechanical stress[14] or ligand–receptor interactions.[15–17] The thermochromic properties of these materials are of particular significance, which in the case of PDA typically manifests itself as a color change from blue to red upon heating. Amphiphilic diacetylene monomers (DA) in aqueous solutions tend to form supramolecular structures as a result of the self-organization process, such as vesicles,[18] nanoplatlets,[19] nanofibers,[20] thin films[21] and also supramolecular crystals.[22] A favorable geometrical and orientational arrangement, referred to as the Schmidt criterion, satisfying conditions such as the appropriate distance between the two reactive carbon atoms of DA monomers (4.9 Å), as well as the angle with respect to the acetylene axis (45°) makes it possible to produce polydiacetylenes by topochemical

[a] Faculty of Chemistry, Jagiellonian University, Gronostajowa 2, 30-387, Krakow, Poland. E-mail: tomasz.uchacz@uj.edu.pl, s.zapotoczny@uj.edu.pl
[b] Doctoral School of Exact and Natural Sciences, Jagiellonian University, Lojasiewicza 11, 30-348 Krakow, Poland
[c] Academic Centre for Materials and Nanotechnology, AGH University of Krakow, A. Mickiewicza 30 St., 30-059 Krakow, Poland
[d] Key Lab of Science and Technology of Eco-textile, Ministry of Education, College of Chemistry and Chemical Engineering, Donghua University, Shanghai 201620, China
[e] State Key Laboratory for Modification of Chemical Fibers and Polymer Materials, College of Chemistry and Chemical Engineering & Center for Advanced Low-dimension Materials, Donghua University, 2999 North Renmin Road, Shanghai 201620, China

† Electronic supplementary information (ESI) available. See DOI: https://doi.org/10.1039/d5tc01233c

polymerization.[23] PDA is obtained by the addition reaction of 1,4 diacetylene monomers under 254 nm UV light, γ-ray irradiation[24] or plasma induction,[25] forming alternate bonds in the en-yn polymer chain.[26] It is this delocalized network of π electrons that gives PDA its peculiar optical properties. Polymerization leads to a blue phase of PDA exhibiting a characteristic absorption peak with a maximum at around 640 nm, which is usually monitored by UV-Vis spectrophotometry. When the materials are exposed to an external stimulus, the absorption peak shifts hypsochromically to ∼540 nm which is described as the red phase of PDA. Visible to the naked eye, the color change from blue to red and the change in the absorption peak are related to the modification of the energy value required to shift π electrons to the LUMO molecular orbital (PDA transition to the red phase) from the HOMO orbital (PDA transition from the blue phase). In addition, PDA in the red phase is characterized by the lowest excited state with B_u symmetry, which produces strong fluorescence with a peak at about 650 nm as a result of the radiation decay.[27] In the case of the blue phase of PDA, the lowest excited state has A_g symmetry, which is dipole forbidden, thus showing very weak fluorescence.[28] The mechanism of the color change has still not received a full explanation. A number of studies indicate that conformational changes in macromolecules play a significant role in thermochromism disrupting the effective conjugation length in the chain. In addition, evidence from Raman spectroscopy studies supports the assumption that PDA alkyl chains adopt a *trans* conformation in the blue phase, and under the influence of a stimulus switch to a *gauche* conformation in the red phase.[29] Moreover, the report on mechanochromism of polydiacetylenes showed that the blue-to-red transformation is caused by shear forces exerted perpendicularly to the PDA backbone.[30] This suggests that the release of mechanical stresses acting on the side chains during polymerization is the main factor responsible for thermal color transitions.[31]

Thermochromism of most PDA-based assemblies is usually irreversible while for some applications reversibility is highly desirable.[32–34] An effective strategy for the fabrication of PDA systems with reversible thermochromism is to modify the headgroups of monomers by forming intra- and inter-chain or aromatic interactions, as well as changing the terminal carboxyl groups. The resulting stronger π–π interactions or hydrogen bonds in the chain backbone can control the colorimetric reversibility of PDA-based materials, as well as modulate the temperature range over which such a transition occurs.[35–37] Recent studies indicate that an important feature of PDA with reversible thermochromic properties is the existence of an intermediate state in which electronic relaxation of PDA occurs, as shown by analysis of frequency-resolved transient absorption signals.[38]

Modification of the side chain and main vesicle group of PDA strongly affects the colorimetric response to temperature changes. The longer the side chain, the stronger the interactions in the inter- and intra-chain dispersion of the polylayer, resulting in a slower color change in response to the stimulus. It turns out that the number of methylene units in the linker and hydrophobic tail of PDA is also important in the color recovery ability.[39,40] However, despite its many positive aspects, chemical modification involves many complicated synthetic procedures. Due to their small size and large surface area, nanoparticles are increasingly used as nanosubstrates in self-assembly processes. Their properties enable the effective anchoring of various functional groups, promoting the formation of organized nanocomposite structures. Interactions between the active chemical groups on the nanoparticle surface and the functional groups in organic materials lead to the formation of stable, ordered systems, where key roles are played by interactions such as hydrogen bonding, electrostatic interactions, and van der Waals forces. These organizational processes significantly affect the physicochemical properties of nanocomposites, including their ability to undergo reversible temperature changes, which can result in substantial modification of the material's thermal parameters.[41] Recent studies also show that self-assembly is positively enhanced by the generation of electrostatic interactions between metal cations and negatively charged carboxyl groups of PDA derivatives. This can be achieved by embedding such cations as Zn^{2+}, Ca^{2+}, Li^{+}, Na^{+} and Cs^{+} into the structure.[42–44] Dimensionality is also important in the development of PDA-based colorimetric sensing systems. For example, zero-dimensional PDA liposomes did not provide any response comparable to that of one-dimensional nanofibers, which are able to form efficient connection sites with matrices leading to smart chromatic materials.[45]

The thermochromic reversibility of polydiacetylenes can be controlled by changing the internal amide functional groups in the monomers, as well as the linker structures of the amide groups.[46,47] This enhances the interaction of PDA chains by forming multiple hydrogen bonds. It has been shown that the temperature as well as the reversibility of the process is related to the number and corresponding orientation of the groups forming the hydrogen bonds. Moreover, the reversible temperature range might be increased by incorporation of modified PDA derivatives into an appropriately selected matrix rich in hydrogen bond interactions. An example of a matrix compound is the sodium salt of alginic acid.[48,49] Alginate (Alg) is a natural copolysaccharide whose linear chain is built of D-mannuronate and L-guluronate segments.[50] This natural polymer swells relatively quickly in water and has unique gelation properties with respect to monovalent and divalent ions. Appropriate selection of the gelation period and gelling agents that are tailored to the matrix may increase the efficiency of the PDA-based hydrogel sensor.[51] By dispersing thermochromic derivatives of PDA in hydrogel platforms, advanced composite materials can be created through *e.g.*, wet spinning, resulting in smart polymer fibers that meet the demands of modern sensors.[52] Furthermore, it is important to emphasize that the crosslinking of alginate with Ca^{2+} ions is a reversible and facile process that does not require elevated temperatures or toxic reagents.[53] This makes it highly suitable for the encapsulation of sensitive biological or chemical components. Additionally, alginate hydrogels exhibit excellent permeability to small molecules and ions, which is essential for enabling a dynamic sensor response to changes in the

environment, and concentration of analytes. The use of calcium as the crosslinking agent not only facilitates the rapid and spatially controlled formation of a stable gel network but also enables modulation of the hydrogel's stiffness and porosity by adjusting the solution composition. This approach allows for the fine-tuning of the mechanical and transport properties of the sensor to meet the demands of specific applications. Thus, calcium-crosslinked alginate hydrogels represent a promising platform for the development of modern soft sensors that combine the advantages of biodegradable and renewable materials with high functionality and precisely tailored performance characteristics.[54]

In this paper, we show that appropriate modification of PDA may induce the formation of 2D conjugated nanostructures that can be incorporated into a polymer matrix leading to a new material with improved reversibility of thermochromic behavior. PDA-based 2D nanostructures (nanoplatelets) exhibit enhanced surface area as compared to 3D structures that is advantageous for their potential sensing applications but is commonly advantageous also with respect to mechanical properties or enhanced interactions with the functional groups of the matrix polymer. As a starting compound, we selected 10,12-pentacosadiynoic acid (PCDA), which, compared to the frequently studied 10,12-tricosadiylic acid, provides a greater response to an external stimulus due to its longer hydrophobic chain. It was modified to introduce more hydrogen bond forming groups that should affect both interactions between the monomer units and enhance the integration of the formed self-assembled conjugated nanostructures in the polymer matrix. We selected sodium alginate (Alg) as a matrix for the formation of thermochromic nanocomposites as a common gel-forming polymer that does not require thermal treatment during gelation, while the proposed approach may also be used for other polymer matrices that can form hydrogen bonds.

Experimental

Materials

10,12-Pentacosadiynoic acid (PCDA, ≥97% HPLC), *N*-(2-aminoethyl)acetamide (technical grade, 90%), ethyl-3-(3-dimethylaminopropyl)carbodiimide hydrochloride (EDCl, for synthesis), *N*-hydroxysuccinimide (NHS, 98%), chloroform-d ($CDCl_3$, ≥99.8 atom% D), water (H_2O-HPLC, suitable for HPLC), calcium chloride ($CaCl_2$, anhydrous, granular, ≤7.0 mm, ≥93.0%), and alginic acid sodium salt (Alg) from brown algae were all purchased from and delivered by Sigma-Aldrich (St. Louis, MO, USA). Dichloromethane (DCM, 99.8%, extra dry) was purchased from Acros Organics (Geel, Belgium). Chloroform (CH_3Cl, amylene as stabilizer), sodium chloride (NaCl), magnesium sulphate ($MgSO_4$, anhydrous pure p.a.), and ethyl acetate (AcOEt, pure p.a.) were purchased from Chempur (Piekary Slaskie, Poland). Silicon with natural silicon oxide layer (polished wafer: BORON/THK 625 ± 15 μm/Res 10.0–20.0, Onsemi, Czech Republic) was used as substrates.

Methods

Synthesis of *N*-(2-acetamidoethyl)pentacosa-10,12-diynamide (PCDA-NH). PCDA (400 mg, 1.07 mmol) was introduced into a pressure reactor filled with 10 mL of anhydrous DCM. The mixture was placed in an ice bath and *N*-(2-aminoethyl)acetamide (1.17 mmol), EDCl (2.78 mmol) and NHS (2.78 mmol) were added. The reaction mixture was stirred overnight at room temperature and the process was terminated by adding 20 mL of ice-cold water. After that, the reaction mixture was extracted with AcOEt, NaCl(aq) and dried over anhydrous $MgSO_4$. Combined organic layers were evaporated under reduced pressure to provide the desired product as a white solid (349.8 mg; 71.4%). ^{1}H NMR (400 MHz, $CDCl_3$); δ (ppm): 6.30 (s, 1H), 6.18 (s, 1H), 3.38 (dt, J = 4.8, 3.4 Hz, 4H), 2.22 (t, J = 7.0 Hz, 4H), 2.16 (t, J = 7,6 Hz, 2H), 1.97 (s, 3H), 1.61–1.39 (m, 32 H), 0.86 (t, J = 6.9 Hz, 3 H). ^{13}C NMR (101 MHz, $CDCl_3$); δ (ppm): 174.70, 171.49, 77.73, 77.54, 65.36, 65.27, 40.53, 40.13, 36.75, 32.00, 29.73, 29.71, 29.69, 29.56, 29.43, 29.25, 29.22, 29.18, 28.99, 28.95, 28.83, 28.43, 28.36, 25.72, 23.30, 22.77, 19.29, 19.26, 14.22. HRMS (ESI+): 458.3761.

Formation of nanostructures based on PCDA or PCDA-NH. 3.75 mg (0.01 mmol) of PCDA or 4.59 mg (0.01 mmol) of PCDA-NH was dissolved in 10 mL of CH_3Cl, then filtered through a 0.45 μm H-PTFE syringe filter into a vial. The solvent was then evaporated with a stream of argon to form a film at the bottom of the vial, and then 20 mL of H_2O-HPLC or Alg aqueous solution (0.01%, 0.001% or 0.0001%) was added, followed by pulsed sonication (pulse 2 s, pause 2 s) for 15 minutes using a 3 mm diameter sonication probe (Sonics Vibracell 130 W) (Newtown, CT, USA) set at 60% of the maximum power. The obtained dispersion (final concentration of PCDA or PCDA-NH equal to 0.5 mM) was left in a fridge at 4 °C for 18 h and then exposed to 254 nm hand-held lamps (Intensity: 0.25 mW cm^{-2}) for 3 min to photopolymerize the diacetylene groups. The nanostructures thus produced were named respectively: dispersion in water (PCDA-3D, PCDA-NH-2D), dispersion in: 0.01% Alg (PCDA-NH-2D-Alg-0.01%), 0.001% Alg (PCDA-NH-2D-Alg-0.001%), 0.0001% Alg (PCDA-NH-2D-Alg-0.0001%).

Preparation of the dispersion of PCDA-NH nanostructures in alginate gel. 0.2 g of Alg was added to 10 ml of a 0.5 mM dispersion of PCDA-NH in a 0.001% Alg solution, reaching a final concentration of Alg of about 2% (m/v). The mixture prepared in this way (PCDA-NH-2D-Alg) was sonicated for 3 min and then poured evenly into a Petri dish and poured over a 2% (m/v) $CaCl_2$ solution to completely cover the Alg solution. After 10 min, the gel was transferred to another Petri dish filled with 2% (m/v) $CaCl_2$ solution for another 10 min. The formed gel (PCDA-NH-2D-Gel) was then washed with distilled water. Both PCDA-NH-2D-Gel and PCDA-NH-2D-Alg were irradiated at 254 nm for 3 min using a hand-held lamp before further measurements.

Apparatus and methods. Nuclear magnetic resonance (NMR) spectra were recorded using Jeol 400 (^{1}H NMR at 400 MHz and ^{13}C NMR at 101 MHz). Chemical shifts (δ) were reported in ppm and coupling constants (J) in Hz. All chemical shifts were analyzed in reference to the solvent residual signal of $CDCl_3$.

FTIR spectra were recorded using a Nicolet iS10 spectrometer with an MCT/A detector (Thermo Fisher ScientificTM, Waltham, MA, USA) with an ATR accessory (Smart iTX) applied (number of scans: 128, range: 750–3500 cm^{-1}, resolution: 4 cm^{-1}, gain: 2.0).

HRMS analysis was performed using a MicroTOF II mass spectrometer (Bruker, Bremen, Germany) equipped with the time of flight (TOF) analyzer. The MS detection was performed using the positive ion mode (ESI+), and the profile spectra were acquired within the mass range of 50–3000 *m/z*. The ESI conditions were as follows: nebulizer pressure 0.4 bar, dry gas 4.0 L min^{-1} heated up to 180 °C, and capillary voltage −4500 V. Mass calibration was carried out using sodium formate clusters according to the procedure given by a manufacturer. Data were collected by Compass DataAnalysis 3.2 software (Bruker). Expected ions attributed to analytes were predicted by the IsotopicPattern software (Bruker, Germany). Prior to the analysis samples were dissolved in chloroform (≥99.8%, Sigma-Aldrich).

Atomic force microscopy (AFM) topography images were obtained on a Dimension Icon microscope (Bruker, Santa Barbara, CA, USA) operating in air in PeakForce Tapping (PFT) QNM® mode, using standard silicon cantilevers with a nominal elastic constant of 0.4 N m^{-1}, a triangular tip geometry and a nominal tip radius of 2 nm. Samples were prepared by applying a drop of the appropriate aqueous dispersion onto a silicon wafer (previously cleaned by sonication for 30 min in isopropanol), and then blowing off the solution with an argon stream.

UV-Vis absorption spectra were measured in a quartz cuvette 1QS2 or 21QS10 (Biosens, Warszawa, Poland) at various temperatures using a U-2900 dual-beam spectrophotometer (Hitachi, Tokyo, Japan). For solution measurements, cuvettes with an optical path of 10 mm were used, while for gel measurements cuvettes with an optical path of 2 mm were used. Parts of appropriately cut gel were placed in such a cuvette that was later filled with H_2O-HPLC. The spectra were measured with 800 nm min^{-1} scan speed and 1.0 nm sampling interval then smoothened and baseline-corrected.

Zeta potentials were measured for the dispersions of nanostructures without any dilution at 25 °C with a Zetasizer Nano Series instrument (Malvern Instruments, Malvern, UK). Dynamic light scattering (DLS) measurements were performed using the same instrument and measurement conditions. The reported data represent the averages from three series of measurements (10–100 runs each).

The colorimetric response to temperature changes was recorded using a TRACER FHD WEB007 USB-A webcam (resolution: 1920 × 1080; 30 frames per second). The actual temperature was measured using an electronic thermometer with thermocouple sticking to the surface of the studied gel. For the measurements of a wet gel sample it was placed between two microscope glass slides that were sealed with scotch tape. This system was then placed on a hot plate of a magnetic stirrer. A dry gel sample was heated locally with a blow of hot air delivered through a glass tube from a heat gun. In both cases the samples were cooled down to room temperature spontaneously after switching off the heaters. The frames from the video were analyzed using the RGB analyzer built into ImageJ software (open source license).

CHARMM-GUI[55] and Packmol[56] software were used to create initial 8 × 8 bilayer systems with a 45 Å thick layer of water molecules (TIP3P – model) and also with a 50 Å thick layer of sodium alginate aqueous solution (16 alginate chains, 12 mers each) above and under the bilayer (see further for the details of the system). CHARMM general force fields provided the force field for the PCDA-NH model and classical molecular dynamics (MD) were performed using the LAMMPS[57] (large-scale atomic/molecular massively parallel simulator). Utilizing the conjugate gradients approach, the system was initially reduced. The Lennard-Jones potential used to represent van der Waals interactions had a cutoff radius of 12 Å, and force-switching began at 10 Å. The long-range particle-particle-mesh approach was used to account for electrostatic interactions with 10^{-6} accuracy. After the system had been pretreated, MD simulations were run for 6.5 ns in water and 8 ns for the system in Alg solution. For further calculations only the data after stabilization of the total energy (1.5 ns for water and 4.0 ns for Alg solution) were considered. The thickness of the PCDA-NH bilayer was determined by analyzing the average density profile of nitrogen atoms along the *z*-axis, using 4 Å intervals. The absolute thickness was calculated as the distance between the points on the *z*-axis where the nitrogen atom density reached 10% of its maximum value.

Differential scanning calorimetry (DSC) measurements were performed using a Q20 instrument (TA Instruments, New Castle, DE, USA) equipped with alumina crucibles. DSC measurements were performed according to the following temperature program: I heating: Ramp 5.00 °C min^{-1} to 80.00 °C; I cooling: Ramp 5.00 °C min^{-1} to 30.00 °C; II heating: Ramp 5.00 °C min^{-1} to 80.00 °C; II cooling Ramp 5.00 °C min^{-1} to 30.00 °C. The measurements were performed in a controlled inert gas atmosphere (gas flow 100 mL min^{-1}) with a heating/cooling rate β = 5 °C min^{-1}.

Powder diffraction data were collected using a Malvern Panalytical Empyrean Series 3 diffractometer in Bragg–Brentano (reflection) mode. A copper X-ray source (λ = 1.5419 Å) and a GaliPIX3D detector were employed for all measurements. The sample was placed in a sample holder within an Anton Paar TTK 600 non-ambient chamber, and the following temperature program was applied, with diffraction measurements performed at each temperature: 298 K, then in the cycle 288–323–288 K in 5 K steps, and finally it was heated to 353 K and cooled down to 288 K.

Results and discussion

Synthesis of the PCDA derivative and its self-assembly into nanoplatelets

A PCDA derivative was first synthesized and then its ability to self-organize into nanostructures that exhibit thermochromic behavior was tested (see Fig. 1).

In order to increase the number of groups in the monomer structure capable of forming intermolecular hydrogen bonds,

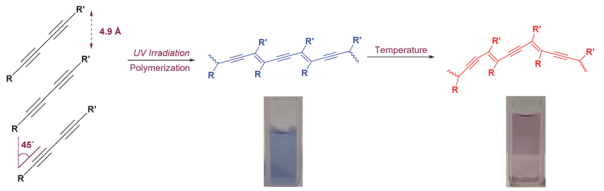

Fig. 1 Schematic presentation of the topochemical polymerization of diacetylenes and their typical color changes after stimulation.

the carboxylic acid group of PCDA was modified by reaction with *N*-(2-aminoethyl)acetamide leading to a new compound with two amide groups (Fig. 2). ^{1}H NMR and ^{13}C NMR spectra of the compound (see the ESI,† Fig. S1 and S2) showed signals at 6.30 and 6.18 ppm, characteristic of the hydrogen atoms of N–H groups, and signals at 174.70 and 171.49 ppm corresponding to the carbon atoms of amides, respectively, confirming successful synthesis of PCDA-NH. This was further corroborated by the FTIR spectroscopy (Fig. S3, ESI†) and HRMS results (Fig. S4, ESI†).

As a result of the application of ultrasound, PCDA self-organized in a solution forming commonly observed vesicles (PCDA-3D). Characterization of the structures formed using PCDA-NH revealed a change in morphology, as a consequence of the modification of end groups of PCDA. The use of sonication led to the generation of nanosheet structures (PCDA-NH-2D), which are likely more favorable for the exploration of mechanochromic or thermochromic properties, due to implied anisotropy.

The formation of spherical structures with a diameter of about 50 nm (Fig. 3a and Fig. S5a, b, ESI†) made of unmodified PCDA, as well as 2D nanostructures made of PCDA-NH (Fig. 3b and Fig. S5c, d, ESI†) was confirmed by AFM (the structures were imaged before photopolymerization). PCDA-NH-2D nanosheets exhibit lateral sizes at the level of several hundred nanometers (200–700 nm) and thicknesses of only 5 nm (Fig. 3b; some additional bilayers are situated on top of each other), which is in accordance with the values observed previously for PCDA-based polymerized bilayers.[58] The plotted height profile of a single nanosheet (Fig. S6a, ESI†) indicates its height of about 5 nm. Based on this, the formation of a PCDA-NH-2D polymer bilayer may be proposed, in which the hydrophilic groups are arranged on surfaces of the formed 2D assemblies. This enables the formation of intermolecular hydrogen bonds while some free head groups are able to form additional hydrogen bonds with the polymer matrix groups (see below for details). To maintain a height of PCDA-NH-2D equal to 5 nm, PCDA-NH hydrophobic chains from two oppositely situated molecules must interpenetrate and interact with each other. The establishment of the aforementioned polymer bilayer ensures that the appropriate

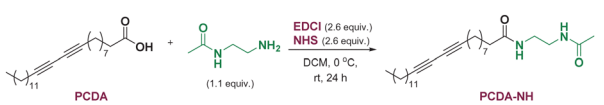

Fig. 2 Scheme for the synthesis of PCDA-NH.

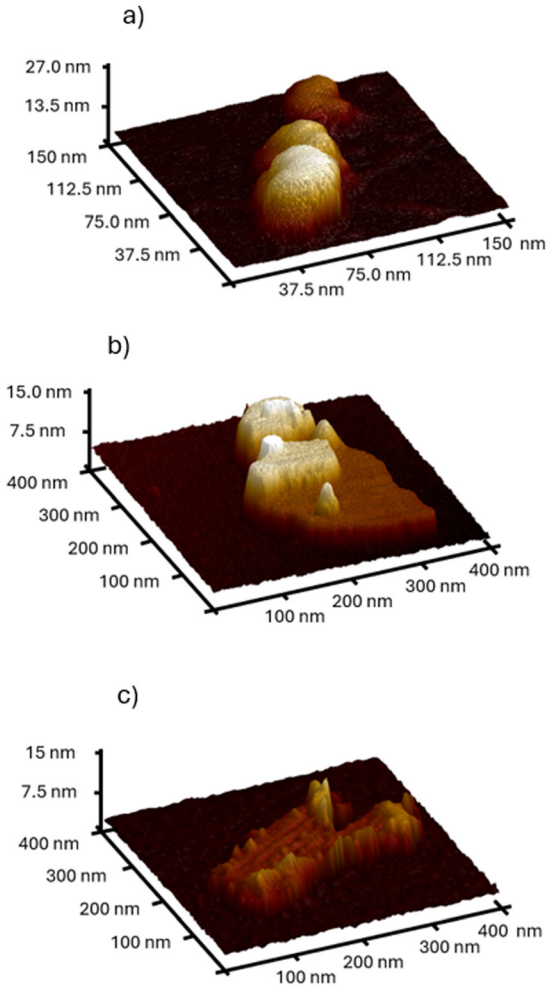

Fig. 3 AFM images in air PCDA-3D (a), PCDA-NH-2D – before polymerization (b), and PCDA-NH-2D – after polymerization (c) deposited on a silicon surface.

distances and angles between adjacent diacetylene groups are maintained, satisfying the Schmidt criterion mentioned earlier. Performing the appropriate topochemical reaction (photopolymerization) enables formation of the system of conjugated bonds (–C=C–C≡C–).

The structures of PCDA-NH-2D after polymerization were also investigated *via* AFM (Fig. 3c). It was observed that polymerization results in compression of the bilayer to a height of approximately 4 nm (Fig. S6b, ESI†) likely due to induced conformational changes.

To validate the architecture of the nanoplatelets imaged by AFM, MD simulations of the bilayer solvated with water molecules were performed (Fig. S7, ESI†).[59–61] The stabilized structures (Fig. S7f and i, ESI†) were analyzed to check the density of nitrogen atoms present in the system. Based on this, the thickness of the bilayer was determined to be equal to 51 Å for the water system and 45 Å for the alginate solution system (Fig. S7c, ESI†), which correlates with the thickness measured using AFM.

XRD data indicate the existence of a crystalline phase. The powder diffraction patterns at room temperature exhibit a

prominent dominant zone effect, with clear 001 (2.212°) and 003 (6.614°) peaks corresponding to an interlayer distance of *ca.* 40 Å (Fig. S8, ESI†). However, the 002 peak is weak and overlaps with a signal from the instrument optics. Both the position (*i.e.*, interlayer distance) and the intensity ratio of the first maxima are consistent with data reported for similar compounds.[62]

Thermochromism of an aqueous dispersion of PCDA-NH-2D

Aqueous dispersions of PCDA-3D and PCDA-NH-2D were exposed to light with a wavelength of 254 nm for a defined period of time (Fig. 4). The solutions changed to a blue color as a result. This observation can be assigned to the formation of –C═C–C≡C– conjugated bonds in the 2D structures due to polymerization of the modified monomer units.

To evaluate how the introduction of the amide groups and implied increase in the number of hydrogen bond interactions affects the reversibility of the thermochromic behavior, a series of temperature-dependent UV-Vis spectra were collected in the 10–50 °C temperature range. The absorption spectra of PCDA-3D (Fig. 5a) and PCDA-NH-2D (Fig. 5b) (after photopolymerization) in the 450–700 nm range were analyzed. It was observed that as the temperature rises, the absorption of the low energy band (550–700 nm; blue form) decreased and the absorption of the higher energy band (450–550 nm; red form) increased for both PCDA-NH-2D and PCDA-3D. However, when the systems were cooled back to 10 °C, only partial recovery of the band at around 640 nm was observed for PCDA-NH-2D, while for PCDA-3D, this blue recovery was so small that the process was considered irreversible.

The reversibility of the process can be quantified based on the absorption spectra as the relative change in "percent blue" (PB) that is defined in eqn (1):[63]

$$\mathrm{PB} = \frac{A_{\mathrm{blue}}}{A_{\mathrm{red}} + A_{\mathrm{blue}}} \times 100\% \quad (1)$$

where A is the absorbance at the maximum of the band characteristic of the blue (A_{blue}) or red (A_{red}) form. It is clear that for the blue form before heating the value of A_{red} measured at around 540 nm is nonzero so the starting PB value is below 100% but it is normalized to this value for clarity of the presentation (Fig. 5c). Analysis of the temperature dependence of PB values revealed that the reversibility of the thermochromic switching of colors is on the level of 7% only for PCDA-3D (Fig. 5c). It was demonstrated that the attachment of the *N*-2-acetamidoethyl group to PCDA and implied increase of the hydrogen bond interaction in PCDA-NH-2D assembly resulted in increases of the PB value to 26% (Fig. 5c). These interactions may disrupt the synclinal conformation adopted by the red

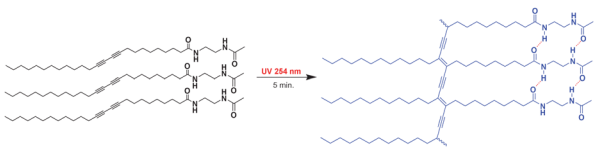

Fig. 4 Schematic photopolymerization within PCDA-NH-2D assembly.

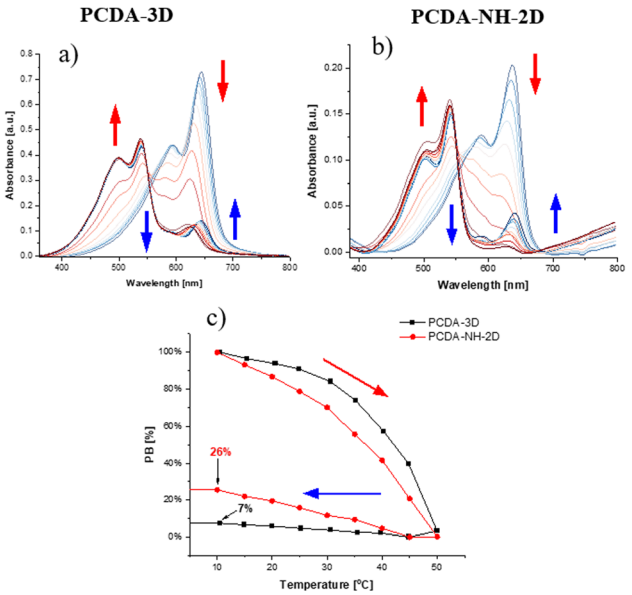

Fig. 5 UV-Vis absorption spectra of aqueous dispersions of PCDA-3D (a) and PCDA-NH-2D (b) during heating (red arrows) and cooling (blue arrows) in the 10–50 °C range and the respective changes of normalized PB (percentage of blue) *versus* temperature (c).

form as a result of maintaining the conjugated bond system in the strained planar conformation of the blue phase.

Temperature-dependent powder diffraction revealed two phase transitions (Fig. S8, ESI†). The first transition, occurring at 318–323 K, results in the formation of another crystalline phase and is reversible. The second transition, observed below 353 K, leads to an amorphous phase and is irreversible. The thermal annealing up to 328 K results in the increased contribution of the crystal phase. Heating at 353 K leads to a completely amorphous phase, but crystallinity is restored after cooling. However, the diffraction resembles the one at 323 K characteristic of the red form. Analogous outcomes were noted for the pure PCDA-NH monomer (Fig. S9, ESI†), suggesting comparable structural alterations for PCDA-NH-2D and PCDA-NH in crystalline form.

In order to determine whether unreacted monomer molecules are still present in the polymerized nanostructures, thermal analyses of the PCDA-NH monomer and PCDA-NH-2D were performed and compared (Fig. S10, ESI†). The results revealed that the phase transition temperature in the polymerized material is lower compared to the monomer form by about 5 °C (with both cooling and heating). Such observations mainly indicate the lack of non-polymerized monomers in the PCDA-NH-2D nanostructures. Based on this, it can be concluded that all monomers were combined to form the polymer structure, indicating that the system was fully cross-linked which also explains its enhanced thermal stability.

Effect of Alg on the thermochromism of PCDA-NH-2D

As mentioned above, PCDA-NH self-organizes into bilayer structures with the inner phase composed of hydrophobic tails. Thus, the hydrophilic heads may be involved not only in mutual

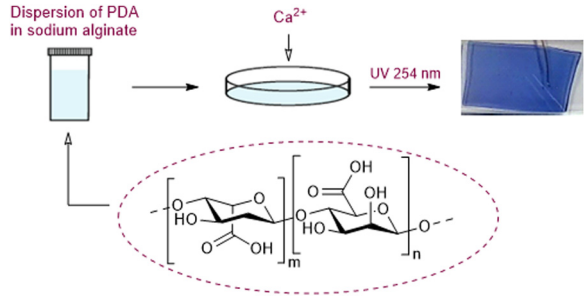

Fig. 6 Procedure for manufacturing alginate gel.

interaction but also in the formation of intermolecular hydrogen bonds with the functional groups of the matrix, in which they can be dispersed. Thus, we applied Alg as a hydrogel matrix of natural origin (Fig. 6). Moreover, developing a stimuli-responsive material by combining a PCDA-NH-based sensory material as the signal-generating component with a responsive hydrogel as the matrix would also broaden its applicability. Due to the high swelling ability of Alg, using it as a matrix should enable the effective transfer of the force of volumetric expansion to the PCDA-NH sensory molecules. In addition, the individual hydrogen bonds of Alg further enhance the interactions which can have a positive effect on increasing the level of colorimetric reversibility.

Thermochromism of PCDA-NH-2D in Alg dispersion

The thermochromic behavior was also studied for dispersions of PCDA-NH-2D in Alg solutions with concentrations of 0.0001%, 0.001%, and 0.01%, before polymerization. UV-Vis spectra were recorded for those dispersions during heating and cooling in the temperature range of 10–50 °C (Fig. S11, ESI†). The highest recovery of the absorption band maximum at 650 nm (blue form) and 550 nm (red form) after heating and subsequent cooling processes were observed for PCDA-NH-2D-Alg-0.001% (Fig. S11b, ESI†).

Following the variations of PB values in the heating–cooling cycle (Fig. 7) one may conclude that reversibility of the thermochromic behavior of PCDA-NH-2D is the best in the 0.001% Alg

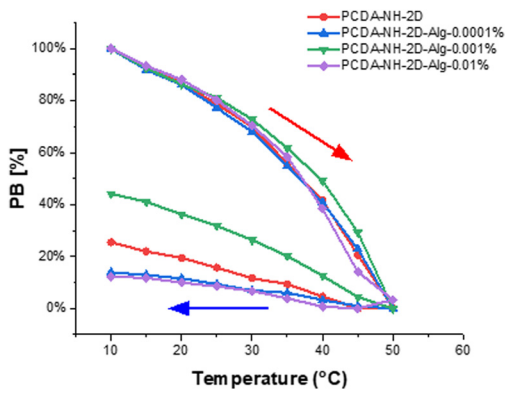

Fig. 7 Changes of normalized PB values for dispersions of PCDA-NH-2D in water and various Alg solutions as determined based on UV-Vis spectra (heating – red arrow; cooling – blue arrow).

medium as recovery of the PB value after cooling was found to be as high as 44% – almost twice higher than in pure water (24%). Interestingly, a significant decrease in colorimetric reversibility was observed for the other two solutions. Reducing the concentration of Alg to 0.0001% leads to a reduction in PB recovery to *ca.* 14%, while for the 0.01% solution the recovery reached only about 12%. To explain these observations zeta potentials were measured for aqueous dispersions of PCDA-3D, PCDA-NH-2D and Alg solution as well as for dispersions of PCDA-NH-2D in Alg solutions (Table S1, ESI†). Similar zeta potential values were obtained for PCDA-NH-2D-Alg-0.001% (−26.5 mV) and PCDA-NH-2D in water (−28.9 mV) indicating the highest stabilities of such dispersions. At both PCDA-NH-2D-Alg-0.01% and PCDA-NH-2D-0.0001% the modules of zeta potential values were smaller: −19.9 mV and −21.7 mV, respectively, that correlate with the greatest stability of the dispersion in 0.001% Alg. In addition, correlograms (DLS measurements) were collected to determine the particle size distribution in the system and their dynamics in the studied medium (Fig. S12a, ESI†). A poor quality correlogram for PCDA-NH-2D particles dispersed in pure water was collected indicating broad distributions of smaller and larger aggregates (Fig. S12b, ESI†), while for the highest Alg concentrations only large aggregates were formed (the shortest correlation times). Reasonable correlograms and respective size distributions were observed for both PCDA-NH-2D-Alg-0.001% and PCDA-NH-2D-Alg-0.0001% but for further studies PCDA-NH-2D-Alg-0.001% was selected due to the highest absorbance of the starting dispersion (Fig. S11b, ESI†) and the mentioned stability issues. It appears that this medium provides adequate conditions for optimum nanosheet–matrix interactions and limiting excessive aggregation. Decreasing the concentration of Alg leads to a reduction of the interactions between Alg and the nanosheets while higher Alg concentrations may increase the chance of "glueing" the nanosheets by macromolecules and result in their flocculation. It is worth mentioning that the calculated (MD simulations) average area occupied by a molecule in the PCDA-NH bilayer in the sodium alginate solution is roughly 10% smaller than in water. This compression may lead to increased stability of the system due to denser packing of the monomers which in turn enables higher conversion of the polymerization and stronger electronic absorption.

Thermochromism of PCDA-NH-2D in crosslinked Alg gel

The formation of nanocomposites containing 2D nanoplatelets in a hydrogel matrix expands the potential applications of such thermochromic systems and also increases the stability and resistance of the material to external conditions. Thus, the obtained dispersion was subjected to gelation by simple addition of a crosslinking solution containing Ca^{2+} ions leading to the formation of PCDA-NH-2D-Gel. To evaluate the effect of the divalent ion on the thermochromism of the system, the temperature-dependent UV-Vis absorption spectra were recorded for PCDA-NH-2D-Alg (Fig. 8a) and PCDA-NH-2D-Gel (Fig. 8b). In both cases, a similar trend in the red and blue bands, as observed previously for PCDA-NH-2D (Fig. 5b), was noticed.

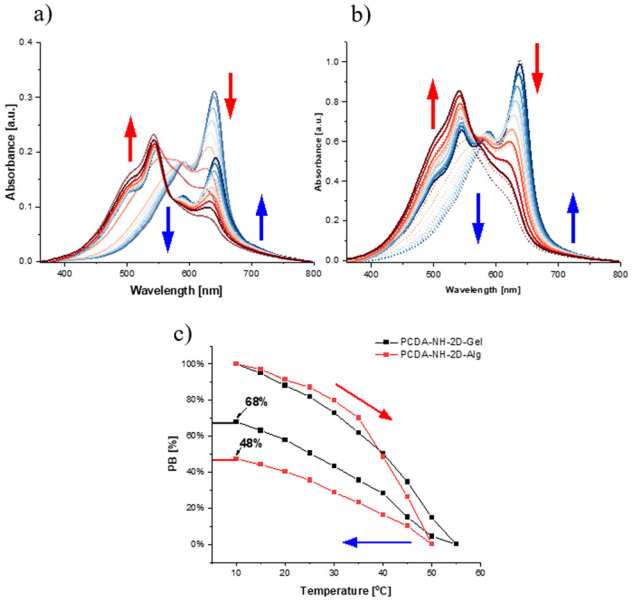

Fig. 8 UV-Vis absorption spectra of PCDA-NH-2D-Alg (a) and PCDA-NH-2D-Gel (b) during heating (red arrows) and cooling (blue arrows) in the 10–50 °C range and the respective changes of normalized PB values *versus* temperature (c). For clarity regarding (b), the spectra captured during heating are drawn with a dotted line and solid lines indicate the spectra captured during cooling.

However, the degree of recovery of the blue band after the cooling was significantly enhanced, especially for the cross-linked PCDA-NH-2D-Gel sample. Furthermore, the thermal shift of the wavelength was not observed indicating restoration of the system after a heating–cooling cycle that is structurally similar to the native one. However, the red form also remains populated after cooling as the respective band does not disappear. This reversibility seems to be enhanced thanks to integration of the nanoplatelets in the polymer matrix through hydrogen bonds. Gelation using Ca^{2+} further strengthens the immobilization of the nanoplatelets and integration within the polymer matrix. This seems to promote the restoration of primary hydrogen bonds in the absence of thermal disorder. The changes of PB during the heating–cooling cycle (Fig. 8c) indicated that for the uncrosslinked PCDA-NH-2D-Alg system the recovery of PB was found to be 48%, while it substantially increased to 68% for the cross-linked system (PCDA-NH-2D-Gel).

It is likely that in the uncrosslinked Alg, during heating the dispersed nanoplatelets, in addition to internal rearrangement, may migrate leading to some aggregates after subsequent cooling. In the nanocomposite hydrogel such spontaneous movement is limited, which reduces the likelihood of aggregation of PCDA-NH-2D nanoplatelets that implies different local environments for thermoresponsive nanostructures. These observations strongly support the hypothesis on the correlation between the number and strength of intermolecular hydrogen bonds and the degree of colorimetric reversibility of the PCDA-based materials.[64]

Dispersed PCDA-NH-2D nanosheets in cross-linked Alg were subjected to measurements of their colorimetric response to temperature changes. Hydrogel fragments of appropriate sizes were subjected to heating and subsequent spontaneous cooling processes, which was recorded as movies (see the ESI,† Movies S1 and S2). The analysis of the thermochromism in PCDA-NH-2D-Gel (Fig. 9a) and PCDA-NH-2D-GelDry (Fig. 9b) was performed on the basis of the time-lapsed images. Histograms showing the distribution of colors in the collected images were prepared. They depict the number of pixels corresponding to each component in the three-dimensional RGB space (R-red, G-green and B-blue). The final color of the material is the resultant of these three components. Based on histograms

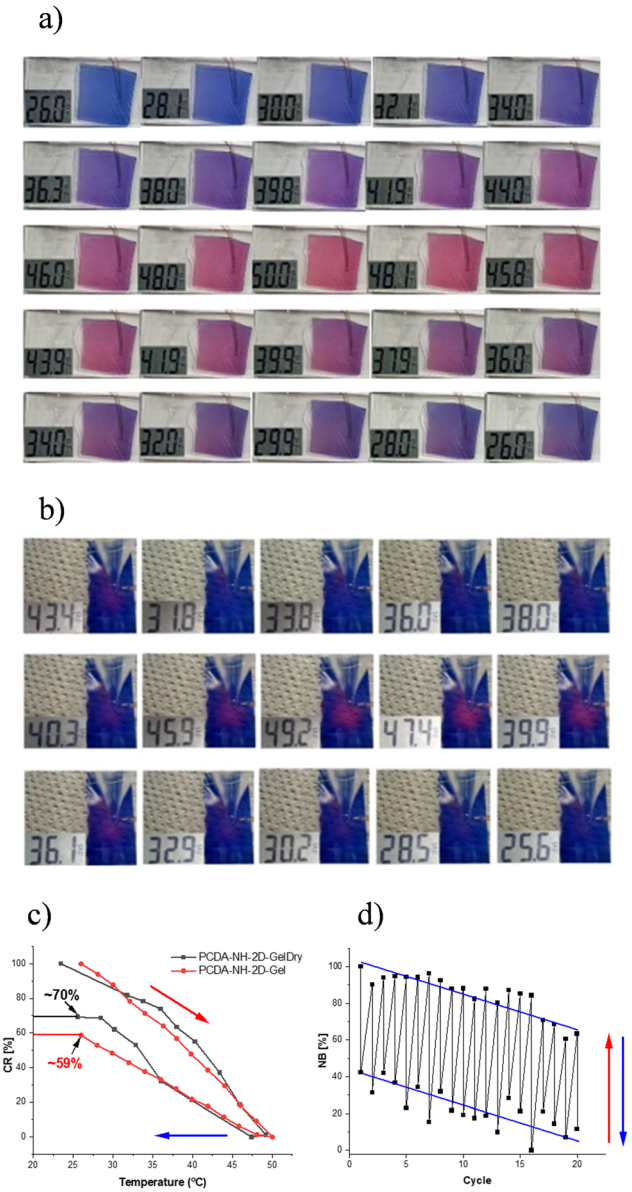

Fig. 9 Visual observation of wet PCDA-NH-2D-Gel (a) and dry PCDA-NH-2D-GelDry (b) samples during heating and subsequent cooling; the temperature transition curves (dependence of normalized CR on temperature changes) for PCDA-NH-2D-Gel and PCDA-NH-2D-GelDry (c); dependence of normalized NB on the heating–cooling cycles for PCDA-NH-2D-GelDry (d).

obtained from the photographs of PCDA-NH-2D-Gel (Fig. S13a, ESI†), it was determined that both the brightness and the number of blue pixels are the highest. At 50 °C, there is an increase in the intensity and frequency of red pixels (Fig. S13b, ESI†). When the wet gel is cooled to the initial temperature (26 °C), the intensity of the blue color is not fully recovered, and the green color reaches its highest pixel frequency (Fig. S13c, ESI†). However, the brightness of the blue pixels is still the highest, which may indicate the predominance of blue in the final color of the sample. In the case of PCDA-NH-2D-GelDry, already in the histogram determined for the initial temperature we observe a small contribution of the red pixels (Fig. S14a, ESI†). At 50 °C, there is an increase, however, compared to the dry gel, and it is close to the value of the intensity of the blue color pixels (Fig. S14b, ESI†). Cooling PCDA-NH-2D-GelDry results in compensation of red and green pixels with simultaneous restoration of the intensity and reduction of the frequency of blue pixels (Fig. S14c, ESI†). As a result, the PCDA-NH-2D-GelDry takes on a blue color which is a noticeable change compared to the dark purple coloration of the PCDA-NH-2D-Gel.

The colorimetric response (CR) characterizes the percentage conversion to the red phase at a given temperature and time, which is the proportion of blue color in the total color of the material and can be calculated using eqn (2):

$$\mathrm{CR} = \frac{\mathrm{Blue_{mean}}}{\mathrm{Red_{mean}} + \mathrm{Blue_{mean}}} \times 100\% \qquad (2)$$

where $\mathrm{Blue_{mean}}/\mathrm{Red_{mean}}$ is the final percentage of blue/red color (mean contribution of blue/red channel in the RGB histogram) after thermochromic transition. Thus, for an ideal colorimetric response of the material CR = 100%. The colorimetric response of the heating–cooling cycle for the wet and dry gel (Fig. 9c) was determined based on the images in Fig. 9a and b. The final CR value obtained after cooling the gel to the initial temperature determines the degree of reversibility. Based on the CR curves, it was shown that the reversibility of the process for PCDA-NH-2D-Gel was 59% while for PCDA-NH-2D-GelDry an increase in CR value to 70% was observed. It seems that embedding the thermochromic nanosheets into the matrix strongly interacting with them helps to restore the original conformation and backbone strains after the heating/cooling cycle. The observed differences between dry and wet gel may be explained taking into account various contents of water. The presence of water in the Alg matrix may provide larger freedom of movement of PCDA-NH-2D nanosheets as compared to the dry gel. What is more, better integration of the nanosheets with the matrix can be achieved if less water molecules competing for the formation of hydrogen bonds with the nanoplatelets is present in the nanocomposite. In addition, the change in the colorimetric response of the dry gel as a function of the heating–cooling cycle was followed (Fig. 9d). For that purpose, the normalized value of the percentage of blue (NB) in the three-dimensional space consisting of red, green and blue colors, was calculated following eqn (3):

$$\mathrm{NB} = \frac{\mathrm{Blue_{mean}}}{\mathrm{Red_{mean}} + \mathrm{Green_{mean}} + \mathrm{Blue_{mean}}} \times 100\% \qquad (3)$$

Moreover, it showed that the percentage of blue in relation to red and green was monotonically decreasing with successive heating/cooling cycles but the difference between NB values for the heated and cooled gel remained practically constant between successive cycle. This reflects the fact that the blue band can be perfectly restored after the heating/cooling (see Fig. 8b for comparison), while the residual red band builds up in each cycle.

Conclusions

We presented here novel nanocomposite materials composed of thermochromic PCDA-based nanostructures embedded in an alginate matrix that exhibit enhanced reversibility of thermochromic behavior. This was achieved by appropriate modification of PCDA molecules using (*N*-aminoethyl)acetamide that resulted in the introduction of amide groups capable of forming hydrogen bonds stabilizing the desired interaction. Such obtained PCDA-NH were shown to self-assemble into 2D nanosheets (PCDA-NH-2D) with 5 nm thickness, typical for bilayers, and a few hundred nanometers in lateral dimensions as determined by AFM. Molecular modeling was also performed confirming the proposed architectures of PCDA-NH-2D while for native PCDA only spherical vesicles were observed. Based on the analysis of UV-Vis absorption spectra of the dispersions of thermochromic nanostructures, we showed that the introduction of an amide group into the polydiacetylene-based monomer (PCDA-NH) increased the restoration of the original blue color in the self-assembled nanostructures after heating/cooling cycles from 7% for PCDA-3D to 26% for PCDA-NH-2D as measured using a ''percent blue'', PB, parameter. This can be attributed to the stabilizing effect of numerous hydrogen bonds formed between PCDA-NH molecules in the 2D nanostructure. XRD and DSC measurements for PCDA-NH-2D indicated the existence of a crystalline phase, as well as the absence of non-polymerized PCDA-NH monomers in the mixture. Importantly, the presence of alginate polymer (Alg) in the dispersion further increased the reversibility of thermochromic behavior reaching PB = 44% for the dispersion of PCDA-NH-2D in 0.001% Alg. This indicated that the nanoplatelets can be further stabilized by Alg, which is capable of forming intermolecular hydrogen bonds with PCDA-NH-2D. Moreover, cross-linking the system using Ca^{2+} as a gelling agent increased the degree of blue band reversibility to 68%. In this case, gelation seems to lead not only to immobilization of the nanoplates but also to their limited aggregation that could otherwise drive the whole nanocomposite to irreversible thermochromic behavior. In such loosely bound fillers the interactions with the matrix would be not sufficient to restore the original conformation and backbone strains in the thermochromic nanoplatelets after heating/cooling cycles. The highest reversibility of the

thermochromic behavior was demonstrated in dry crosslinked gel for which the colorimetric response (the parameter determined from the image analysis) reached a very high value of 70%. This can be attributed to the formation of even stronger hydrogen bonds between PCDA-NH-2D and carboxylic groups in the Alg matrix due to the lower contribution of interactions with water molecules allowing the restoration of the original intermolecular hydrogen bonds PCDA-NH-2D to the greatest extent leading to original conformation and backbone strains defining the blue form. The formed nanocomposite material is characterized by incomplete colorimetric reversibility. While the chromatic response is not fully reversible over multiple heating–cooling cycles, we consider this feature to be an advantageous characteristic in the context of developing smart sensing platforms. Specifically, the reproducible difference between the initial and final colorimetric states of the material after each thermal cycle remains consistent, which enables the use of this shift as a reliable indicator of cumulative thermal exposure. This property opens up the possibility of designing sensors that not only respond to temperature changes in real time but also serve as cumulative thermal history indicators, effectively reporting the degree of material fatigue or thermal degradation. This kind of feature is particularly valuable in applications where monitoring the lifespan or operational safety of thermally sensitive components is critical. Our colorimetric response (CR) analysis was based on the evaluation of optical images captured using a standard camera. Importantly, this imaging-based approach can be easily implemented using widely available mobile devices, such as smartphones, without the need for specialized instrumentation. This provides a cost-effective, accessible, and user-friendly method for material diagnostics, enabling end users to perform *in situ* assessments of material performance or wear using open-source or commercially available applications. Moreover, we have identified that the transition from reversible to irreversible thermochromic behavior occurs beyond a critical threshold temperature of approximately 60–70 °C. This delineation provides a clearly defined operational window for safe and reversible sensor function, beyond which irreversible changes serve as a built-in thermal warning or damage signal. In summary, the partial irreversibility of the thermochromic response not only does not limit the usability of the material but actually extends its functional relevance by enabling the detection of material wear and thermal stress accumulation. The integration of this feature with simple imaging tools supports the development of next-generation, low-cost, and broadly accessible diagnostic systems for industrial, environmental, or biomedical applications.

Author contributions

Karolina Bieniaś: methodology, formal analysis, investigation, and writing – original draft; Piotr Wieczorek: methodology, formal analysis, investigation, and writing – original draft; Tomasz Uchacz: methodology, formal analysis, supervision, and writing – review & editing; Alicja Fryc: investigation; Angelika Kmita: investigation; Xueling Feng: writing – review & editing; Peiyi Wu: writing – review & editing and funding acquisition; Szczepan Zapotoczny: conceptualization, writing review & editing, supervision, funding acquisition, and project administration.

Conflicts of interest

There are no conflicts to declare.

Data availability

The raw/processed data required to reproduce the findings of these studies are available in JU RODBUK repository (**https://doi.org/10.57903/UJ/6EDERL**).

Acknowledgements

This work was financially supported by the National Science Center (NCN) in Poland (project no. UMO-2021/40/Q/ST5/00164). This study was carried out using the research infrastructure cofunded by the European Union in the framework of the Smart Growth Operational Program, Measure 4.2; Grant No. POIR.04.02.00-00-D001/20, "ATOMIN 2.0 – ATOMic scale science for the INnovative economy". We gratefully acknowledge the Polish high-performance computing infrastructure PLGrid (HPC Center: ACK Cyfronet AGH) for providing computer facilities and support within computational grant no. PLG/2024/017061. This research was supported by a grant from the Faculty of Chemistry under the Strategic Programme Excellence Initiative at Jagiellonian University. The open-access publication of this article has been supported by a grant from the Faculty of Chemistry under the Strategic Programme Excellence Initiative at Jagiellonian University.

References

1 M. J. A. Shin, Color-Detectable Vitamin C Controlled-Release System Fabricated Using Electrospinning, *Polymers*, 2024, **16**(10), 1347.
2 A. Bhattacharjee, R. Clark, C. Gentry-Weeks and Y. V. Li, A Novel Receptor-FreePolydiacetylene Nanofiber Biosensor for Detecting: E. Coli via Colorimetric Changes, *Mater. Adv.*, 2020, **1**(9), 3387–3397.
3 H. Shin, B. Yoon, I. S. Park and J. M. Kim, An Electrothermochromic Paper Display Based on Colorimetrically Reversible Polydiacetylenes, *Nanotechnology*, 2014, **25**(9), 094011.
4 P. Liu, W. Chang, L. Ju, L. Chu, Z. Xie, J. Chen and J. Yang, Bioinspired Noniridescent Structural Color with Hidden Patterns for Anticounterfeiting, *ACS Appl. Nano Mater.*, 2019, **2**(9), 5752–5760.
5 F. Bahrami, N. Eslahi and R. Jahanmardi, Electrospinning of Smart Nanofibers Based on PVP/PDA for Wound Dressing Applications, *J. Text. Inst.*, 2023, **115**(10), 1865–1877.
6 W. Lu, G. Wu, L. Gan, Y. Zhang and K. Li, Functional Fibers/Textiles for Smart Sensing Devices and Applications in Personal Healthcare Systems, *Anal. Methods*, 2024, **16**(31), 5372–5390.

7 Y. Zhao, A. D. Slepkov, C. O. Akoto, R. McDonald, F. A. Hegmann and R. R. Tykwinski, Synthesis, Structure, and Nonlinear Optical Properties of Cross-Conjugated Perphenylated Iso-Polydiacetylenes, *Chem. - Eur. J.*, 2005, **11**(1), 321–329.
8 G. Wegner, Tochemical Reactions of Monomers with Conjugated Triple Bonds, *Z. Naturforsch.*, 1969, **24b**(7), 824–832.
9 C. P. de Oliveira, N. F. Ferreira Soares, A. V. N. de Carvalho Teixeira, T. V. de Oliveira and A. M. Maradini Filho, Biomimetic System Characterization: PH-Induced Chromatic Transition and Nanostructural Transformation of Polydiacetyle and Dimyristoylphosphatidylcholine Vesicles Under PH Variation Using Dynamic Light Scattering (DLS) Technique, *J. Food Chem. Nanotechnol.*, 2019, **05**(03), 65–69.
10 J. Huo, Z. Hu, G. He, X. Hong, Z. Yang, S. Luo, X. Ye, Y. Li, Y. Zhang, M. Zhang, H. Chen, T. Fan, Y. Zhang, B. Xiong, Z. Wang, Z. Zhu and D. Chen, High Temperature Thermochromic Polydiacetylenes: Design and Colorimetric Properties, *Appl. Surf. Sci.*, 2017, **423**, 951–956.
11 C. Khanantong, N. Charoenthai, S. Wacharasindhu, M. Sukwattanasinitt, W. Yimkaew, N. Traiphol and R. Traiphol, Achieving Reversible Thermochromism of Bisdiynamide Polydiacetylene *via* Self-Assembling in Selected Solvents, *Colloids Surf., A*, 2020, **603**, 125225.
12 S. S. Shin, D. Y. Kim, K. Bae, H. Kang, S. J. Ha, A. Patil, J. M. Kim and B. J. Park, Optical Laser Tweezer-Directed Single Particle Solvatochromism of Conjugated Polydiacetylene, *Small Struct.*, 2024, 2400171.
13 X. Chen, L. Hong, X. You, Y. Wang, G. Zou, W. Su and Q. Zhang, Photo-Controlled Molecular Recognition of α-Cyclodextrin with Azobenzene Containing Polydiacetylene Vesicles, *Chem. Commun.*, 2009, 1356–1358.
14 A. R. Burns, R. W. Carpick, D. Y. Sasaki, J. A. Shelnutt and R. Haddad, Shear-Induced Mechanochromism in Polydiacetylene Monolayers, *Tribol. Lett.*, 2001, **10**(1–2), 89–96.
15 Q. Huang, W. Wu, K. Ai and J. Liu, Highly Sensitive Polydiacetylene Ensembles for Biosensing and Bioimaging, *Front. Chem.*, 2020, **8**, 1–21.
16 Y. Li, L. Wang, Y. Wen, B. Ding, G. Sun, T. Ke, J. Chen and J. Yu, Constitution of a Visual Detection System for Lead(II) on Polydiacetylene-Glycine Embedded Nanofibrous Membranes, *J. Mater. Chem. A*, 2015, **3**(18), 9722–9730.
17 B. Hu and P. Wu, An Ultrathin Polydiacetylene Nanosheet as Dual Colorimetric and Fluorescent Indicator for Lysophosphatidic Acid, a Cancer Biomarker, *Giant*, 2020, **3**, 100025.
18 J. S. Miller, T. J. Finney, E. Ilagan, S. Frank, Y. Chen-Izu, K. Suga and T. L. Kuhl, Fluorogenic Biosensing with Tunable Polydiacetylene Vesicles, *Biosensors*, 2025, **15**(1), 1–22.
19 J. Oh, I. Jeon, D. Kim, Y. You, D. Baek, S. J. Kang and J. Lee, Highly Stable Upconverting Nanocrystal-Polydiacetylenes Nanoplates for Orthogonal Dual Signaling-Based Detection of Cyanide, *ACS Appl. Mater. Interfaces*, 2020, **12**(4), 4934–4943.
20 G. Graf, S. Drescher, A. Meister, V. M. Garamus and A. Blume, Nanofiber Formation and Polymerization of Bolalipids with Diacetylene-Modified Single Alkyl Chains, *J. Phys. Chem. B*, 2019, **123**(7), 1566–1577.
21 R. Sergi, B. Brugnoli, E. Sturabotti, A. Piozzi, L. Galantini, V. Taresco and I. Francolini, Colorimetric Transition of Polydiacetylene/Cyclodextrin Supramolecular Assemblies and Implications as Colorimetric Sensors for Food Phenolic Antioxidants, *Macromol. Chem. Phys.*, 2023, **224**(16), 1–11.
22 J. Seo, J. F. Joung, S. Park, Y. J. Son, J. Noh and J. M. Kim, Light-Directed Trapping of Metastable Intermediates in a Self-Assembly Process, *Nat. Commun.*, 2020, **11**(1), 1–9.
23 G. M. J. Schmidt, Photodimerization in the Solid State, *Pure Appl. Chem.*, 1971, **27**(4), 647–678.
24 X. Sun, T. Chen, S. Huang, L. Li and H. Peng, Chromatic Polydiacetylene with Novel Sensitivity, *Chem. Soc. Rev.*, 2010, **39**(11), 4244–4257.
25 S. Lee, Y. Cho, B. U. Ye, J. M. Baik, M. H. Kim and J. Yoon, Unprecedented Colorimetric Responses of Polydiacetylenes Driven by Plasma Induced Polymerization and Their Patterning Applications, *Chem. Commun.*, 2014, **50**(83), 12447–12449.
26 X. Yu, C. MuYu, H. Xu, J. Zhao and G. Yang, Recent Progress in the Design of Conjugated Polydiacetylenes with Reversible Thermochromic Performance: A Review, *Polym. Chem.*, 2023, **14**(19), 2266–2290.
27 B. G. Zoltan Sow, Fluorescence and Excited-State Structure of Conjugated Polymers, *Adv. Mater.*, 1994, **280**(4), 280–287.
28 J. S. Filhol, J. Deschamps, S. G. Dutremez, B. Boury, T. Barisien, L. Legrand and M. Schott, Polymorphs and Colors of Polydiacetylenes: A First Principles Study, *J. Am. Chem. Soc.*, 2009, **131**(20), 6976–6988.
29 I. S. Park, H. J. Park, W. Jeong, J. Nam, Y. Kang, K. Shin, H. Chung and J. M. Kim, Low Temperature Thermochromic Polydiacetylenes: Design, Colorimetric Properties, and Nanofiber Formation, *Macromolecules*, 2016, **49**(4), 1270–1278.
30 L. Juhasz, R. D. Ortuso and K. Sugihara, Quantitative and Anisotropic Mechanochromism of Polydiacetylene at Nanoscale, *Nano Lett.*, 2021, **21**(1), 543–549.
31 R. W. Carpick, D. Y. Sasaki and A. R. Burns, First Observation of Mechanochromism at the Nanometer Scale, *Langmuir*, 2000, **16**(3), 1270–1278.
32 M. Weston, A. H. Pham, J. Tubman, Y. Gao, A. D. Tjandra and R. Chandrawati, Polydiacetylene-Based Sensors for Food Applications, *Mater. Adv.*, 2022, **3**(10), 4088–4102.
33 H. Xing, Y. Song, L. Ma, F. Wang, M. Zhang, Z. Li, Z. Wan, X. Cui and G. Yang, Preparation of Bis-Polydiacetylene with Reversible Thermochromism and High Sensitivity toward Pb^{2+} Detection, *ACS Appl. Polym. Mater.*, 2024, **6**, 24.
34 S. Kingchok, P. Nontasorn, K. Laohhasurayotin, N. Traiphol and R. Traiphol, Reversible Thermochromic Polydiacetylene/Zinc-Aluminium Layered Double Hydroxides Nanocomposites for Smart Paints and Colorimetric Sensors: The Crucial Role of Zinc Ions, *Colloids Surf., A*, 2021, **610**, 125733.
35 J. Seo, C. Kantha, J. F. Joung, S. Park, R. Jelinek and J. M. Kim, Covalently Linked Perylene Diimide–Polydiacetylene Nanofibers Display Enhanced Stability and Photocurrent with Reversible FRET Phenomenon, *Small*, 2019, **15**(19), 1–8.

36 M. I. Khazi, C. Balachandra, G. Shin, G. H. Jang, T. Govindaraju and J. M. Kim, Co-Solvent Polarity Tuned Thermochromic Nanotubes of Cyclic Dipeptide-Polydiacetylene Supramolecular System, *RSC Adv.*, 2020, **10**(58), 35389–35396.

37 B. Hu, S. Sun, B. Wu and P. Wu, Colloidally Stable Monolayer Nanosheets with Colorimetric Responses, *Small*, 2019, **15**(5), 1–7.

38 J. Baek, J. F. Joung, S. Lee, H. Rhee, M. H. Kim, S. Park and J. Yoon, Origin of the Reversible Thermochromic Properties of Polydiacetylenes Revealed by Ultrafast Spectroscopy, *J. Phys. Chem. Lett.*, 2016, **7**(2), 259–265.

39 S. Ampornpun, S. Montha, G. Tumcharern, V. Vchirawongkwin, M. Sukwattanasinitt and S. Wacharasindhu, Odd-Even and Hydrophobicity Effects of Diacetylene Alkyl Chains on Thermochromic Reversibility of Symmetrical and Unsymmetrical Diyndiamide Polydiacetylenes, *Macromolecules*, 2012, **45**(22), 9038–9045.

40 J. Qi, Y. Kim, K. Takahashi, K. Aoki, I. Hisaki, T. Nakamura and N. A. Tamaoki, Series of Bisamide-Substituted Diacetylenes Exhibiting a Terminal Alkyl Odd/Even Parity Effect on Mechanoactivated Photopolymerization, *Chem. - Eur. J.*, 2021, **27**(11), 3832–3841.

41 N. Traiphol, N. Rungruangviriya, R. Potai and R. Traiphol, Stable Polydiacetylene/ZnO Nanocomposites with Two-Steps Reversible and Irreversible Thermochromism: The Influence of Strong Surface Anchoring, *J. Colloid Interface Sci.*, 2011, **356**(2), 481–489.

42 N. Traiphol, A. Chanakul, A. Kamphan and R. Traiphol, Role of Zn^{2+} Ion on the Formation of Reversible Thermochromic Polydiacetylene/Zinc Oxide Nanocomposites, *Thin Solid Films*, 2017, **622**, 122–129.

43 P. Zheng, B. Ding, R. Shi, Z. Jiang, W. Xu, G. Li, J. Ding and X. Chen, A Multichannel Ca^{2+} Nanomodulator for Multilevel Mitochondrial Destruction-Mediated Cancer Therapy, *Adv. Mater.*, 2021, **33**(15), 1–11.

44 X. Huang, S. Jiang and M. Liu, Metal Ion Modulated Organization and Function of the Langmuir-Blodgett Films of Amphiphilic Diacetylene: Photopolymerization, Thermochromism, and Supramolecular Chirality, *J. Phys. Chem. B*, 2005, **109**(1), 114–119.

45 S. Seo, J. Lee, M. S. Kwon, D. Seo and J. Kim, Stimuli-Responsive Matrix-Assisted Colorimetric Water Indicator of Polydiacetylene Nanofibers, *ACS Appl. Mater. Interfaces*, 2015, **7**(36), 20342–20348.

46 S. Wacharasindhu, S. Montha, J. Boonyiseng, A. Potisatityuenyong, C. Phollookin, G. Tumcharern and M. Sukwattanasinitt, Tuning of Thermochromic Properties of Polydiacetylene toward Universal Temperature Sensing Materials through Amido Hydrogen Bonding, *Macromolecules*, 2010, **43**(2), 716–724.

47 O. Mapazi, P. K. Matabola, R. M. Moutloali and C. J. A. Ngila, Urea-Modified Polydiacetylene-Based High Temperature Reversible Thermochromic Sensor: Characterisation and Evaluation of Properties as a Function of Temperature, *Sens. Actuators, B*, 2017, **252**, 671–679.

48 W. Wang, C. Xiang, Q. Liu, M. Li, W. Zhong, K. Yan and D. Wang, Natural Alginate Fiber-Based Actuator Driven by Water or Moisture for Energy Harvesting and Smart Controller Applications, *J. Mater. Chem. A*, 2018, **6**(45), 22599–22608.

49 X. N. Zhang, Y. J. Wang, S. Sun, L. Hou, P. Wu, Z. L. Wu and Q. Zheng, A Tough and Stiff Hydrogel with Tunable Water Content and Mechanical Properties Based on the Synergistic Effect of Hydrogen Bonding and Hydrophobic Interaction, *Macromolecules*, 2018, **51**(20), 8136–8146.

50 A. Sutton, G. E. Harrison, T. E. F. Carr and D. Barltrop, Reduction in the Absorption of Dietary Strontium in Children by an Alginate Derivative, *Int. J. Radiat. Biol.*, 1971, **19**(1), 79–85.

51 S. Song, H. Jang, W. Jeong, J. Shim, S. M. Kim and T. J. Jeon, Thermohypersensitive Polydiacetylene Vesicles Embedded in Calcium-Alginate Hydrogel Beads, *Korean J. Chem. Eng.*, 2023, **40**(2), 398–404.

52 S. Seo, J. Lee, M. S. Kwon, D. Seo and J. Kim, Stimuli-Responsive Matrix-Assisted Colorimetric Water Indicator of Polydiacetylene Nanofibers, *ACS Appl. Mater. Interfaces*, 2015, **7**(36), 20342–20348.

53 R. Wilkońska, P. Bernard, J. Odrobińska-Baliś, W. Wilkoński and S. Zapotoczny, Introduction to Medicinal Chemistry: Synthesis and Investigation of Cross-Linked Alginate Beads with Embedded Micelles as Model Carriers of Hydrophobic Drugs, *J. Chem. Educ.*, 2025, **102**(5), 2190–2196.

54 M. Cibinel, G. Pugliese, D. Porrelli, L. Marsich and V. Lughi, Recycling Alginate Composites for Thermal Insulation, *Carbohydr. Polym.*, 2021, **251**, 116995.

55 S. Jo, T. Kim, V. G. Iyer and W. Im, CHARMM-GUI: A Web-based Graphical User Interface for CHARMM, *J. Comput. Chem.*, 2008, **29**, 1859–1865.

56 L. Martínez, R. Andrade, E. G. Birgin and J. M. Martínez, Packmol: A package for building initial configurations for molecular dynamics simulations, *J. Comput. Chem.*, 2009, **30**(13), 2157–2164.

57 A. P. Thompson, H. M. Aktulga, R. Berger, D. S. Bolintineanu, W. M. Brown, P. S. Crozier, P. J. in 't Veld, A. Kohlmeyer, S. G. Moore, T. D. Nguyen, R. Shan, M. J. Stevens, J. Tranchida, C. Trott and S. J. Plimpton, LAMMPS – a flexible simulation tool for particle-based materials modeling at the atomic, meso, and continuum scales, *Comput. Phys. Commun.*, 2022, **271**, 10817.

58 H. Younesi Araghi and M. F. Paige, Deposition and Photopolymerization of Phase-Separated Perfluorotetradecanoic Acid-10,12-Pentacosadiynoic Acid Langmuir-Blodgett Monolayer Films, *Langmuir*, 2011, **27**(17), 10657–10665.

59 S. Jo, T. Kim, V. G. Iyer and W. Im, CHARMM-GUI: A Web-Based Graphical User Interface for CHARMM, *J. Comput. Chem.*, 2008, **29**, 1859–1865.

60 L. Martínez, R. Andrade, E. G. Birgin and J. M. M. Birgin, Packmol: A Package for Building Initial Configurations for Molecular Dynamics Simulations, *J. Comput. Chem.*, 2009, **30**(13), 2157–2164.

61 A. P. Thompson, H. M. Aktulga, R. Berger, D. S. Bolintineanu, W. M. Brown, P. S. Crozier, P. J. in't

Veld, A. Kohlmeyer, S. G. Moore, T. D. Nguyen, R. Shan, M. J. Stevens, J. Tranchida, C. Trott and S. J. Plimpton, LAMMPS - a Flexible Simulation Tool for Particle-Based Materials Modeling at the Atomic, Meso, and Continuum Scales, *Comput. Phys. Commun.*, 2022, **271**, 108171.

62 J. Pang, L. Yang, B. F. McCaughey, H. Peng, H. S. Ashbaugh, C. J. Brinker and Y. Lu, Thermochromatism and Structural Evolution of Metastable Polydiacetylenic Crystals, *J. Phys. Chem. B*, 2006, **110**(14), 7221–7225.

63 S. Okada, S. Peng, W. Spevak and D. Charych, Color and Chromism of Polydiacetylene Vesicles, *Acc. Chem. Res.*, 1998, **31**(5), 229–239.

64 H. Y. Sagong, M. H. Son, S. H. Min and Y. K. Jung, Controllable color change of polydiacetylene vesicles under thermal-photo stimuli, *Polymer*, 2021, **223**, 124211.

